

AEDC-TR-79-13

OCT 31 1979

NOV 18 1980

MAY 17 1982

JUN 9 1988

cy.2



VORTICITY-STREAM FUNCTION FORMULATION OF COMPRESSIBLE AND INCOMPRESSIBLE TURBULENT INTERNAL FLOWS

John C. Chien

ARO, Inc., a Sverdrup Corporation Company

**ENGINE TEST FACILITY
ARNOLD ENGINEERING DEVELOPMENT CENTER
AIR FORCE SYSTEMS COMMAND
ARNOLD AIR FORCE STATION, TENNESSEE 37389**

**TECHNICAL REPORTS
FILE COPY**

May 1979

**PROPERTY OF U.S. AIR FORCE
AEDC TECHNICAL LIBRARY**

Final Report for Period September 1977 — September 1978

Approved for public release; distribution unlimited.

Prepared for

**ARNOLD ENGINEERING DEVELOPMENT CENTER/DOTR
ARNOLD AIR FORCE STATION, TENNESSEE 37389**

*Property of U. S. Air Force
AEDC LIBRARY
F40600-77-C-0093*

NOTICES

When U. S. Government drawings, specifications, or other data are used for any purpose other than a definitely related Government procurement operation, the Government thereby incurs no responsibility nor any obligation whatsoever, and the fact that the Government may have formulated, furnished, or in any way supplied the said drawings, specifications, or other data, is not to be regarded by implication or otherwise, or in any manner licensing the holder or any other person or corporation, or conveying any rights or permission to manufacture, use, or sell any patented invention that may in any way be related thereto.

Qualified users may obtain copies of this report from the Defense Documentation Center.

References to named commercial products in this report are not to be considered in any sense as an indorsement of the product by the United States Air Force or the Government.

This report has been reviewed by the Information Office (OI) and is releasable to the National Technical Information Service (NTIS). At NTIS, it will be available to the general public, including foreign nations.

APPROVAL STATEMENT

This report has been reviewed and approved.


ELTON R. THOMPSON

Project Manager, Research Division
Directorate of Test Engineering

Approved for publication:

FOR THE COMMANDER



ROBERT W. CROSSLEY, Lt Colonel, USAF
Acting Director of Test Engineering
Deputy for Operations

UNCLASSIFIED

20. ABSTRACT (Continued)

addition to the conventional Poisson-type pressure equation, a new pressure equation with both first- and second-order terms was derived from the momentum equations. A vector path function is included in the pressure equation to improve convergence and accuracy. Applications to a model wind tunnel diffuser and a sudden expansion diffuser are discussed. Good agreement with available experimental data is observed in terms of the pressure coefficient and the length of the recirculation region.

UNCLASSIFIED

PREFACE

The work reported herein was conducted by the Arnold Engineering Development Center (AEDC), Air Force Systems Command (AFSC). The results of the research were obtained by ARO, Inc., AEDC Division (a Sverdrup Corporation Company), operating contractor for the AEDC, AFSC, Arnold Air Force Station, Tennessee, under ARO Project Number E32A-P0A. The Air Force program manager was Mr. Elton R. Thompson. The manuscript was submitted for publication on January 15, 1979.

CONTENTS

	<u>Page</u>
1.0 INTRODUCTION	5
2.0 THE VORTICITY-STREAM FUNCTION FORMULATION	5
3.0 THE PRESSURE EQUATION	6
3.1 The Conventional Pressure Equation	7
3.2 A New Pressure Equation	8
4.0 A TWO-EQUATION k - ϵ TURBULENCE MODEL	12
5.0 BOUNDARY CONDITIONS AND INLET CONDITIONS	13
6.0 NUMERICAL METHOD AND COORDINATE TRANSFORMATION	
6.1 Coordinate Transformation	14
6.2 Initial Flow-Field Guess	15
6.3 Numerical Solution Procedure	17
7.0 RESULTS AND DISCUSSION	
7.1 Incompressible Wind Tunnel Diffuser Flow Computation	17
7.2 Compressible Laminar Flow in a Sudden Expansion Diffuser	22
8.0 CONCLUDING REMARKS	24
REFERENCES	24

ILLUSTRATIONS

Figure

1. Decomposition of Initial Velocity Profiles	16
2. Flow Chart for Incompressible Flow Solution Procedure	18
3. Flow Chart for Compressible Flow Solution Procedure	18
4. 16T Diffuser Geometry	19
5. C_p Distribution for 16T Model Diffuser	20
6. Convergence Characteristics for 16T Model Diffuser Computation	21
7. Convergence Characteristics for the New Pressure Equation	21
8. Velocity and Streamline Distribution of a Sudden Expansion Diffuser	23
9. Convergence Characteristics of Sudden Expansion Diffuser Computation	23

NOMENCLATURE	25
--------------------	----

1.0 INTRODUCTION

Turbulent ducted flow is commonly found in diffusers, nozzles, test cells, and wind tunnels. The complexity of the flow involved depends upon many factors such as the geometry of the wall, the turbulent nature of the flow, flow separation, three-dimensional effects, the Mach number effect, etc.

For incompressible turbulent flow, a method (Refs. 1 and 2) has been developed to obtain the finite-difference solution of the Navier-Stokes equations with a two-equation $k-\epsilon$ turbulence model. It has been used in the computation of both separated and nonseparated turbulent diffuser flows with nonuniform inlet conditions. The original analysis was formulated for two-dimensional (2-D) or axisymmetrical flows with a single-wall boundary layer and a coordinate transformation. In order to handle general nonsymmetrical 2-D flows and annular diffuser flows, another wall boundary layer and coordinate transformation were added to the analysis in the present study. With this modification, a fairly general class of ducted flow problems can now be computed easily with the incompressible Navier-Stokes code. Among other important changes are (1) a simple exponential coordinate transformation to handle the two boundary layers, (2) a formula for the initial flow-field guess, and (3) a new approach for computing the pressure field.

For the compressible flow computations, the requirement to calculate the density variation makes it necessary to know the temperature and pressure fields. It is the purpose of the present study to extend the incompressible analysis to the compressible flow regime within the framework of the vorticity-stream function formulation of the Navier-Stokes equations. The derivation of the governing equations in terms of the vorticity and the stream function, the coordinate transformations, the logic of the numerical procedure, and some preliminary results are presented.

2.0 THE VORTICITY-STREAM FUNCTION FORMULATION

The basic governing equations are the continuity, momentum, and energy equations. The set of steady-state equations can also be expressed in terms of the vorticity and the stream function. These are given in both 2-D Cartesian and cylindrical coordinates as follows (different vorticity-stream function formulations can be found in Refs. 3 and 4):

Vorticity Equation

$$\left(\frac{\partial^2 \Omega}{\partial x^2} + \frac{\partial^2 \Omega}{\partial r^2} \right) - \frac{1}{(\mu + \mu_t)} \left\{ \left(\rho u - 2 \frac{\partial \mu_t}{\partial x} \right) \frac{\partial \Omega}{\partial x} + \left[\rho v - 2 \frac{\partial \mu_t}{\partial r} - \delta \cdot \frac{(\mu + \mu_t)}{r} \right] \frac{\partial \Omega}{\partial r} \right\}$$

$$\begin{aligned}
 & - \left\{ \delta \cdot \frac{\Omega}{(\mu + \mu_t)} \left[\frac{1}{r} \frac{\partial \mu_t}{\partial r} - \frac{(\mu + \mu_t)}{r^2} + \frac{\rho v}{r} \right] + \frac{1}{(\mu + \mu_t)} \left[\frac{\partial \rho}{\partial r} \frac{\partial}{\partial x} \left(\frac{u^2 + v^2}{2} \right) - \frac{\partial \rho}{\partial x} \frac{\partial}{\partial r} \left(\frac{u^2 + v^2}{2} \right) \right] \right. \\
 & + \frac{2}{(\mu + \mu_t)} \frac{\partial \mu_t}{\partial x} \left[\frac{\partial}{\partial r} (\nabla \cdot \vec{v}) \right] - \frac{2}{(\mu + \mu_t)} \frac{\partial \mu_t}{\partial x} \left[\frac{\partial}{\partial x} (\nabla \cdot \vec{v}) \right] \\
 & \left. - \frac{1}{(\mu + \mu_t)} \left[\left(\frac{\partial^2 \mu_t}{\partial x^2} - \frac{\partial^2 \mu_t}{\partial r^2} \right) \left(\frac{\partial v}{\partial x} + \frac{\partial u}{\partial r} \right) + 2 \frac{\partial^2 \mu_t}{\partial x \partial r} \left(\frac{\partial v}{\partial r} - \frac{\partial u}{\partial x} \right) \right] \right\} = 0 \tag{1}
 \end{aligned}$$

where

$$\nabla \cdot \vec{v} = \frac{\partial u}{\partial x} + \frac{\partial v}{\partial r} - \delta \cdot \frac{v}{r}$$

Stream Function Equation

$$\left(\frac{\partial^2 \psi}{\partial x^2} + \frac{\partial^2 \psi}{\partial r^2} \right) - \left(\frac{1}{\rho} \frac{\partial \rho}{\partial x} \right) \frac{\partial \psi}{\partial x} - \left(\frac{1}{\rho} \frac{\partial \rho}{\partial r} + \frac{\delta}{r} \right) \frac{\partial \psi}{\partial r} = -\rho r \delta \Omega$$

where

$$\begin{aligned}
 u & \equiv \frac{1}{\rho r \delta} \frac{\partial \psi}{\partial r} \\
 v & \equiv -\frac{1}{\partial r \delta} \frac{\partial \psi}{\partial x}
 \end{aligned} \tag{2}$$

In the vorticity equation, the first two second-order terms represent the diffusion term, the next two first-order terms represent the convection term, and the rest represent the vorticity source terms. Of the vorticity source terms, the first term comes from the cylindrical coordinates used, the second term is related to the density variation, the next two terms are related to the first-order eddy viscosity variation, and the last term is related to the second-order eddy viscosity variation. The eddy viscosity (μ_t) and the density (ρ) which appear in the vorticity and the stream function equations must be determined from the turbulence modeling, the energy equation, the equation of state, and the pressure equation.

3.0 THE PRESSURE EQUATION

There are several methods available to recover the pressure field, namely (1) by direct integration of the momentum equations, (2) by solving a second-order pressure equation, and (3) by solving a new pressure equation described in the present analysis.

3.1 The Conventional Pressure Equation

In the first approach, it is possible to obtain a pressure field distribution by direct integration of the momentum equation. In the region where the flow variables are relatively smooth and continuous, the pressure integration is straightforward. Otherwise, the local error generated will be carried along the path of integration. As a result, the pressure level at the end of the integration path is usually inaccurate. This happens often along the wall where the velocity gradient is large. This method can be used when the velocity field obtained is accurate and there are enough grid points to define the solution smoothly. The line integration methods used to obtain the pressure distribution, although good for some simple applications, do not generally provide a unique solution.

In the second approach, a Poisson type of pressure equation is derived from the momentum equation through a $(\nabla \cdot)$ operation. The result is a second-order field equation,

$$\left(\frac{\partial^2 p}{\partial x^2} + \frac{\partial^2 p}{\partial r^2} \right) + \frac{\delta}{r} \left(\frac{\partial p}{\partial r} \right) = S_p \quad (3)$$

where

$$\begin{aligned} S_p = & \rho \left[2 \left(\frac{\partial u}{\partial x} \right) \left(\frac{\partial v}{\partial r} \right) - 2 \left(\frac{\partial v}{\partial x} \right) \left(\frac{\partial u}{\partial r} \right) + 2 \frac{\delta \cdot v}{r} \left(\frac{\partial v}{\partial r} + \frac{\partial u}{\partial x} \right) \right] \\ & + \frac{\partial \rho}{\partial x} \left(u \frac{\partial u}{\partial x} - v \frac{\partial u}{\partial r} \right) - \frac{\partial \rho}{\partial r} \left(u \frac{\partial v}{\partial x} + v \frac{\partial v}{\partial r} \right) \\ & - \rho u \frac{\partial}{\partial x} (\nabla \cdot \vec{v}) - \rho v \frac{\partial}{\partial r} (\nabla \cdot \vec{v}) - \rho (\nabla \cdot \vec{v})^2 \\ & + \frac{\partial^2 \mu_t}{\partial x^2} \left[2 \frac{\partial u}{\partial x} - \frac{2}{3} (\nabla \cdot \vec{v}) \right] + \frac{\partial^2 \mu_t}{\partial r^2} \left[2 \frac{\partial v}{\partial r} - \frac{2}{3} (\nabla \cdot \vec{v}) \right] \\ & - \frac{\partial \mu_t}{\partial x} \left[2 \frac{\partial \Omega}{\partial r} + 2 \frac{\delta \cdot \Omega}{r} - \frac{8}{3} \frac{\partial}{\partial x} (\nabla \cdot \vec{v}) \right] \\ & + \frac{\partial \mu_t}{\partial r} \left[2 \frac{\partial \Omega}{\partial x} + 2 \frac{\delta \cdot v}{r^2} + \frac{8}{3} \frac{\partial}{\partial r} (\nabla \cdot \vec{v}) - \frac{2}{3} \frac{\delta}{r} (\nabla \cdot \vec{v}) \right] \\ & + 2 \frac{\partial^2 \mu_t}{\partial x \partial r} \left(\frac{\partial v}{\partial x} + \frac{\partial u}{\partial r} \right) + \frac{4}{3} (\mu + \mu_t) \left[\frac{\partial^2}{\partial x^2} (\nabla \cdot \vec{v}) + \frac{\partial^2}{\partial r^2} (\nabla \cdot \vec{v}) + \frac{\delta}{r} \frac{\partial}{\partial r} (\nabla \cdot \vec{v}) \right] \end{aligned}$$

For 2-D incompressible, constant viscosity flow, Eq. (1) is reduced to the following form:

$$\left(\frac{\partial^2 \bar{p}}{\partial x^2} + \frac{\partial^2 \bar{p}}{\partial r^2} \right) = 2 \left(\frac{\partial u}{\partial x} \frac{\partial v}{\partial r} - \frac{\partial v}{\partial x} \frac{\partial u}{\partial r} \right) \quad (4)$$

where \bar{p} is defined as (p/ρ) .

The second-order pressure equation derived represents an improvement over the direct integration scheme. But there are difficulties associated with the boundary conditions. In most ducted flow problems, the pressure along the wall is not known. For flow between two walls, the zero normal pressure gradient condition would have to be used. As a result, the boundary condition becomes weak in controlling the absolute pressure level. In addition, slow convergence characteristics usually exist for the gradient-type boundary conditions. So far, no satisfactory method has been developed to improve the situation.

3.2 A New Pressure Equation

With the weakness of the second-order pressure equation known, it is possible to create a new pressure equation from the momentum equations with stronger convergence properties. The idea is to retain as much as possible the first-order nature of the momentum equations, while at the same time working with a second-order field equation. Although the approach is highly heuristic, the results of this approach discussed in later sections do support the basic idea. The basic idea behind this new equation is simple and is explained briefly as follows. In most ducted flow problems, there are inviscid and viscous boundary-layer regions. In the subsonic inviscid region, the flow variables change relatively smoothly along the main flow direction (or along the streamline). It is possible to determine a path function in such a way that the resultant pressure equation is highly convective along this path. With proper selection of the coefficient, one can make the second-order diffusion term relatively small. Thus one can achieve the forward integration of the pressure by solving a second-order diffusion-convection pressure equation. In order to obtain the pressure field for the rest of the flow field, one can specify the path function normal to the main flow direction (or normal to the boundary layer).

The pressure equation with this new set of path functions will pick up the pressure information along the main flow direction and propagate it across the boundary layer to reach the wall. This is a natural approach, in a sense, because the normal pressure gradient is usually small. Therefore, one would expect to have relatively accurate pressure distributions. The key to the success is the creation and specification of the vector path function. The new pressure equation derived from the momentum equations with the vector path functions P1 and P2 is as follows:

$$\left(\frac{\partial^2 p}{\partial x^2} + \frac{\partial^2 p}{\partial r^2} \right) + \frac{\delta}{r} \left(\frac{\partial p}{\partial r} \right) - P1 \frac{\rho u_c}{(\mu + \mu_v)} \left(\frac{\partial p}{\partial x} \right) - P2 \frac{\rho u_c}{(\mu + \mu_v)} \left(\frac{\partial p}{\partial r} \right)$$

$$\begin{aligned}
&= 2\rho \left[\left(\frac{\partial u}{\partial x} \right) \left(\frac{\partial v}{\partial r} \right) - \left(\frac{\partial v}{\partial x} \right) \left(\frac{\partial u}{\partial r} \right) + \frac{\delta \cdot v}{r} \left(\frac{\partial v}{\partial r} + \frac{\partial u}{\partial x} \right) \right] \\
&- \frac{\partial \rho}{\partial x} \left(u \frac{\partial u}{\partial x} - v \frac{\partial u}{\partial r} \right) - \frac{\partial \rho}{\partial r} \left(u \frac{\partial v}{\partial x} + v \frac{\partial v}{\partial r} \right) - \rho u \frac{\partial}{\partial x} (\nabla \cdot \vec{v}) - \rho v \frac{\partial}{\partial r} (\nabla \cdot \vec{v}) - \rho (\nabla \cdot \vec{v})^2 \\
&- \frac{\partial^2 \mu_t}{\partial x^2} \left[2 \frac{\partial u}{\partial x} - \frac{2}{3} (\nabla \cdot \vec{v}) \right] + \frac{\partial^2 \mu_t}{\partial r^2} \left[2 \frac{\partial v}{\partial r} - \frac{2}{3} (\nabla \cdot \vec{v}) \right] - \frac{\partial \mu_t}{\partial x} \left[2 \frac{\partial \Omega}{\partial r} + 2 \frac{\delta \cdot \Omega}{r} - \frac{8}{3} \frac{\partial}{\partial x} (\nabla \cdot \vec{v}) \right] \\
&+ \frac{\partial \mu_t}{\partial r} \left[2 \frac{\partial \Omega}{\partial r} + 2 \frac{\delta \cdot \Omega}{r^2} + \frac{8}{3} \frac{\partial}{\partial r} (\nabla \cdot \vec{v}) - \frac{2}{3} \frac{\partial}{\partial r} (\nabla \cdot \vec{v}) \right] + 2 \frac{\partial^2 \mu_t}{\partial x \partial r} \left(\frac{\partial v}{\partial x} + \frac{\partial u}{\partial r} \right) \\
&+ \frac{4}{3} (\mu + \mu_t) \left[\frac{\partial^2}{\partial x^2} (\nabla \cdot \vec{v}) + \frac{\partial^2}{\partial r^2} (\nabla \cdot \vec{v}) + \frac{\delta}{r} \frac{\partial}{\partial r} (\nabla \cdot \vec{v}) \right] \\
&- P1 \frac{\rho u_c}{(\mu + \mu_t)} \left\{ -\rho \left(u \frac{\partial u}{\partial x} + v \frac{\partial u}{\partial r} \right) + \frac{\partial \mu_t}{\partial x} \left[2 \frac{\partial u}{\partial x} - \frac{2}{3} (\nabla \cdot \vec{v}) \right] + \frac{\partial \mu_t}{\partial r} \left(\frac{\partial v}{\partial x} + \frac{\partial u}{\partial r} \right) \right. \\
&\quad \left. + (\mu + \mu_t) \left[-\frac{\partial \Omega}{\partial r} - \delta \frac{\Omega}{r} + \frac{4}{3} \frac{\partial}{\partial x} (\nabla \cdot \vec{v}) \right] \right\} \\
&- P2 \frac{\rho u_c}{(\mu + \mu_t)} \left\{ -\rho \left(u \frac{\partial v}{\partial x} + v \frac{\partial v}{\partial r} \right) + \frac{\partial \mu_t}{\partial x} \left(\frac{\partial v}{\partial x} + \frac{\partial u}{\partial r} \right) + \frac{\partial \mu_t}{\partial r} \left[2 \frac{\partial v}{\partial r} - \frac{2}{3} (\nabla \cdot \vec{v}) \right] \right. \\
&\quad \left. - (\mu + \mu_t) \left[\frac{\partial \Omega}{\partial x} + \frac{4}{3} \frac{\partial}{\partial r} (\nabla \cdot \vec{v}) \right] \right\} \tag{5}
\end{aligned}$$

where P1 and P2 are the vector path functions and u_c is a reference velocity.

The strong convective nature of this new second-order pressure equation is controlled by the path function and the coefficient $[\rho u_c / (\mu + \mu_t)]$. The path function must be specified in advance. It could be changed to improve the accuracy on the basis of the velocity distribution. In general, the path function depends on a particular flow problem to be solved. For the ducted flow application, P1 is one along the centerline or the midposition line and is zero elsewhere. This has an effect of convecting the pressure along the midposition line in the downstream direction. The other path function, P2, is zero along the midposition line, is one in the positive half of the flow field, and is minus one in the lower half of the region. The information about the pressure is then spread away from the midposition line in the normal direction. The underlying physics is explained in the following example:

For a parallel channel flow with a boundary layer and a core region, the new pressure equation behaves in the core region as

$$\left(\frac{\partial^2 p}{\partial x^2}\right) - 1 \cdot \frac{\rho u_c}{\mu} \cdot \left(\frac{\partial p}{\partial x}\right) = S_p \quad (6)$$

On the other hand, in the boundary layer region, it becomes

$$\left(\frac{\partial^2 p}{\partial r^2}\right) - 1 \cdot \frac{\rho u_c}{\mu} \cdot \left\{\frac{\partial p}{\partial r}\right\} = S_p \quad (7)$$

Because of the strong coefficient $(\rho u_c/\mu)$, the pressure field is being convected along the prescribed direction of P1 and P2.

Several obvious advantages can be obtained by using the newly derived pressure equation: (1) the second-order diffusion-convection equation can be easily solved by the general finite-difference formulation with decay function; (2) the path function can be selected in such a way that the error in the pressure field is minimized; (3) a fast convergence rate is realized because of the strong convective nature of the equation; and (4) the problem with the wall boundary condition is relieved because the wall pressure is now approached in the normal-to-the-wall direction.

Some feeling for the complexity of the transformed equation in the computational domain may be gained from the transformed pressure equation shown here.

Transformed Pressure Equation for Compressible Flow

$$\begin{aligned} & \left(\frac{\partial^2 p}{\partial \bar{x}^2}\right) \left(\frac{\partial \bar{x}}{\partial x}\right)^2 + \left(\frac{\partial^2 p}{\partial \bar{r}^2}\right) \left[\left(\frac{\partial \bar{r}}{\partial x}\right)^2 + \left(\frac{\partial \bar{r}}{\partial r}\right)^2\right] - \left(\frac{\partial p}{\partial \bar{x}}\right) \left\{ \left(\frac{\partial^2 \bar{x}}{\partial x^2}\right) + \left(\frac{\partial \bar{x}}{\partial x}\right) \cdot \left[P1 \frac{\rho u_c}{(\mu + \mu_t)}\right] \right\} \\ & - \left(\frac{\partial p}{\partial \bar{r}}\right) \left\{ -\left(\frac{\partial^2 \bar{r}}{\partial x^2}\right) - \left(\frac{\partial^2 \bar{r}}{\partial r^2}\right) - \frac{\delta}{r} \left(\frac{\partial \bar{r}}{\partial r}\right) + \left(\frac{\partial \bar{r}}{\partial x}\right) \left[P1 \frac{\rho u_c}{(\mu + \mu_t)}\right] - \left(\frac{\partial \bar{r}}{\partial r}\right) \left[P2 \frac{\rho u_c}{(\mu + \mu_t)}\right] \right\} \\ & = S_p \end{aligned}$$

where

$$\begin{aligned}
S_p = & -2 \left(\frac{\partial \bar{r}}{\partial x} \right) \left(\frac{\partial \bar{x}}{\partial x} \right) \frac{\partial^2 p}{\partial \bar{x} \partial \bar{r}} + \rho \left\{ 2 \left[\frac{\partial u}{\partial \bar{x}} \left(\frac{\partial \bar{x}}{\partial x} \right) + \frac{\partial u}{\partial \bar{r}} \left(\frac{\partial \bar{r}}{\partial x} \right) \right] \left[\frac{\partial v}{\partial \bar{r}} \cdot \left(\frac{\partial \bar{r}}{\partial r} \right) \right] \right. \\
& - 2 \left[\frac{\partial v}{\partial \bar{x}} \cdot \left(\frac{\partial \bar{x}}{\partial x} \right) + \frac{\partial v}{\partial \bar{r}} \cdot \left(\frac{\partial \bar{r}}{\partial x} \right) \right] \cdot \left[\frac{\partial u}{\partial \bar{r}} \cdot \left(\frac{\partial \bar{r}}{\partial r} \right) \right] + 2 \frac{\delta \cdot v}{r} \cdot \left[(\nabla \cdot \vec{v}) - \delta \cdot \frac{v}{r} \right] \left. \right\} \\
& - \left[\frac{\partial \rho}{\partial \bar{x}} \left(\frac{\partial \bar{x}}{\partial x} \right) + \frac{\partial \rho}{\partial \bar{r}} \cdot \left(\frac{\partial \bar{r}}{\partial x} \right) \right] \cdot \left\{ u \left[\frac{\partial u}{\partial \bar{x}} \cdot \left(\frac{\partial \bar{x}}{\partial x} \right) + \frac{\partial u}{\partial \bar{r}} \cdot \left(\frac{\partial \bar{r}}{\partial x} \right) \right] + v \frac{\partial u}{\partial \bar{r}} \cdot \left(\frac{\partial \bar{r}}{\partial r} \right) \right\} \\
& - \left[\frac{\partial \rho}{\partial \bar{r}} \cdot \left(\frac{\partial \bar{r}}{\partial r} \right) \right] \cdot \left\{ u \left[\frac{\partial v}{\partial \bar{x}} \cdot \left(\frac{\partial \bar{x}}{\partial x} \right) + \frac{\partial v}{\partial \bar{r}} \left(\frac{\partial \bar{r}}{\partial x} \right) \right] + v \frac{\partial v}{\partial \bar{r}} \cdot \left(\frac{\partial \bar{r}}{\partial r} \right) \right\} \\
& - \rho u \left[\frac{\partial}{\partial \bar{x}} (\nabla \cdot \vec{v}) \cdot \left(\frac{\partial \bar{x}}{\partial x} \right) + \frac{\partial}{\partial \bar{r}} (\nabla \cdot \vec{v}) \cdot \left(\frac{\partial \bar{r}}{\partial x} \right) \right] - \rho v \left[\frac{\partial}{\partial \bar{r}} (\nabla \cdot \vec{v}) \cdot \left(\frac{\partial \bar{r}}{\partial r} \right) \right] - \rho (\nabla \cdot \vec{v})^2 \\
& + \left[\frac{\partial^2 \mu_t}{\partial \bar{x}^2} \left(\frac{\partial \bar{x}}{\partial x} \right)^2 + \frac{\partial^2 \mu_t}{\partial \bar{r}^2} \cdot \left(\frac{\partial \bar{r}}{\partial x} \right)^2 + \frac{\partial \mu_t}{\partial \bar{x}} \cdot \left(\frac{\partial^2 \bar{x}}{\partial x^2} \right) + \frac{\partial \mu_t}{\partial \bar{r}} \cdot \left(\frac{\partial^2 \bar{r}}{\partial x^2} \right) + 2 \left(\frac{\partial \bar{r}}{\partial x} \right) \left(\frac{\partial \bar{x}}{\partial x} \right) \frac{\partial^2 \mu_t}{\partial \bar{x} \partial \bar{r}} \right] \\
& \cdot \left\{ 2 \left[\frac{\partial u}{\partial \bar{x}} \cdot \left(\frac{\partial \bar{x}}{\partial x} \right) + \frac{\partial u}{\partial \bar{r}} \cdot \left(\frac{\partial \bar{r}}{\partial r} \right) \right] - \frac{2}{3} (\nabla \cdot \vec{v}) \right\} + \left[\frac{\partial^2 \mu_t}{\partial \bar{r}^2} \cdot \left(\frac{\partial \bar{r}}{\partial r} \right)^2 + \frac{\partial \mu_t}{\partial \bar{r}} \cdot \left(\frac{\partial^2 \bar{r}}{\partial r^2} \right) \right] \cdot \left[2 \frac{\partial v}{\partial \bar{r}} \cdot \left(\frac{\partial \bar{r}}{\partial r} \right) - \frac{2}{3} (\nabla \cdot \vec{v}) \right] \\
& - \left[\frac{\partial \mu_t}{\partial \bar{x}} \left(\frac{\partial \bar{x}}{\partial x} \right) + \frac{\partial \mu_t}{\partial \bar{r}} \left(\frac{\partial \bar{r}}{\partial x} \right) \right] \cdot \left\{ 2 \frac{\partial \Omega}{\partial \bar{r}} \left(\frac{\partial \bar{r}}{\partial r} \right) + 2 \frac{\delta \cdot \Omega}{r} - \frac{8}{3} \left[\frac{\partial}{\partial \bar{x}} (\nabla \cdot \vec{v}) \cdot \left(\frac{\partial \bar{x}}{\partial x} \right) + \frac{\partial}{\partial \bar{r}} (\nabla \cdot \vec{v}) \cdot \left(\frac{\partial \bar{r}}{\partial x} \right) \right] \right\} \\
& + \left[\frac{\partial \mu_t}{\partial \bar{r}} \cdot \left(\frac{\partial \bar{r}}{\partial r} \right) \right] \cdot \left\{ 2 \left[\frac{\partial \Omega}{\partial \bar{x}} \left(\frac{\partial \bar{x}}{\partial x} \right) + \frac{\partial \Omega}{\partial \bar{r}} \cdot \left(\frac{\partial \bar{r}}{\partial x} \right) \right] + 2 \frac{\delta \cdot v}{r^2} + \frac{8}{3} \frac{\partial}{\partial \bar{r}} (\nabla \cdot \vec{v}) \cdot \left(\frac{\partial \bar{r}}{\partial r} \right) - \frac{2}{3} \frac{\delta}{r} (\nabla \cdot \vec{v}) \right\} \\
& + \left\{ \frac{\partial \mu_t}{\partial \bar{r}} \left(\frac{\partial^2 \bar{r}}{\partial x \partial r} \right) + \left(\frac{\partial \bar{r}}{\partial r} \right) \cdot \left[\left(\frac{\partial \bar{x}}{\partial x} \right) \frac{\partial^2 \mu_t}{\partial \bar{x} \partial \bar{r}} + \left(\frac{\partial \bar{r}}{\partial x} \right) \frac{\partial^2 \mu_t}{\partial \bar{r}^2} \right] \right\} \cdot \left\{ 2 \left[\frac{\partial v}{\partial \bar{x}} \cdot \left(\frac{\partial \bar{x}}{\partial x} \right) + \frac{\partial v}{\partial \bar{r}} \left(\frac{\partial \bar{r}}{\partial r} \right) + \frac{\partial u}{\partial \bar{r}} \cdot \left(\frac{\partial \bar{r}}{\partial r} \right) \right] \right\} \\
& + \frac{4}{3} (\mu + \mu_t) \left\{ \left[\frac{\partial^2}{\partial \bar{x}^2} (\nabla \cdot \vec{v}) \cdot \left(\frac{\partial \bar{x}}{\partial x} \right)^2 + \frac{\partial^2}{\partial \bar{r}^2} (\nabla \cdot \vec{v}) \cdot \left(\frac{\partial \bar{r}}{\partial x} \right)^2 + \frac{\partial}{\partial \bar{x}} (\nabla \cdot \vec{v}) \cdot \frac{\partial^2 \bar{x}}{\partial x^2} + \frac{\partial}{\partial \bar{r}} (\nabla \cdot \vec{v}) \cdot \left(\frac{\partial^2 \bar{r}}{\partial x^2} \right) \right. \right. \\
& \quad \left. \left. + 2 \left(\frac{\partial \bar{r}}{\partial x} \right) \left(\frac{\partial \bar{x}}{\partial x} \right) \cdot \frac{\partial^2}{\partial \bar{x} \partial \bar{r}} (\nabla \cdot \vec{v}) \right] + \frac{\delta}{r} \frac{\partial}{\partial \bar{r}} (\nabla \cdot \vec{v}) \cdot \left(\frac{\partial \bar{r}}{\partial r} \right) + \left[\frac{\partial^2}{\partial \bar{r}^2} (\nabla \cdot \vec{v}) \cdot \left(\frac{\partial \bar{r}}{\partial r} \right)^2 \right. \right. \\
& \quad \left. \left. + \frac{\partial}{\partial \bar{r}} (\nabla \cdot \vec{v}) \cdot \left(\frac{\partial^2 \bar{r}}{\partial r^2} \right) \right] \right\}
\end{aligned}$$

$$\begin{aligned}
 & -P1 \frac{\rho u_c}{(\mu + \mu_t)} \cdot \left\{ -\rho u \left[\frac{\partial u}{\partial \bar{x}} \left(\frac{\partial \bar{x}}{\partial x} \right) + \frac{\partial u}{\partial \bar{r}} \left(\frac{\partial \bar{r}}{\partial x} \right) \right] - \rho v \frac{\partial u}{\partial \bar{r}} \cdot \left(\frac{\partial \bar{r}}{\partial r} \right) + \left[\frac{\partial \mu_t}{\partial \bar{x}} \cdot \left(\frac{\partial \bar{x}}{\partial x} \right) + \frac{\partial \mu_t}{\partial \bar{r}} \cdot \left(\frac{\partial \bar{r}}{\partial x} \right) \right] \right. \\
 & \cdot \left\{ 2 \left[\frac{\partial u}{\partial \bar{x}} \cdot \left(\frac{\partial \bar{x}}{\partial x} \right) + \frac{\partial u}{\partial \bar{r}} \cdot \left(\frac{\partial \bar{r}}{\partial x} \right) \right] - \frac{2}{3} (\nabla \cdot \vec{v}) \right\} - \left[\frac{\partial \mu_t}{\partial \bar{r}} \cdot \left(\frac{\partial \bar{r}}{\partial r} \right) \right] \cdot \left\{ \left[\frac{\partial v}{\partial \bar{x}} \cdot \left(\frac{\partial \bar{x}}{\partial x} \right) + \frac{\partial v}{\partial \bar{r}} \cdot \left(\frac{\partial \bar{r}}{\partial x} \right) \right] + \frac{\partial u}{\partial \bar{r}} \cdot \left(\frac{\partial \bar{r}}{\partial r} \right) \right\} \\
 & + (\mu + \mu_t) \cdot \left\{ -\frac{\partial \Omega}{\partial \bar{r}} \cdot \left(\frac{\partial \bar{r}}{\partial r} \right) - \delta \cdot \frac{\Omega}{r} + \frac{4}{3} \left[\frac{\partial}{\partial \bar{x}} (\nabla \cdot \vec{v}) \cdot \left(\frac{\partial \bar{x}}{\partial x} \right) + \frac{\partial}{\partial \bar{r}} (\nabla \cdot \vec{v}) \cdot \left(\frac{\partial \bar{r}}{\partial x} \right) \right] \right\} \\
 & - P2 \frac{\rho u_c}{(\mu + \mu_t)} \cdot \left\{ -\rho u \left[\frac{\partial v}{\partial \bar{x}} \cdot \left(\frac{\partial \bar{x}}{\partial x} \right) + \frac{\partial v}{\partial \bar{r}} \cdot \left(\frac{\partial \bar{r}}{\partial x} \right) \right] - \rho v \frac{\partial v}{\partial \bar{r}} \cdot \left(\frac{\partial \bar{r}}{\partial r} \right) + \left[\frac{\partial \mu_t}{\partial \bar{r}} \cdot \left(\frac{\partial \bar{r}}{\partial r} \right) \right] \right. \\
 & \cdot \left[2 \frac{\partial v}{\partial \bar{r}} \cdot \left(\frac{\partial \bar{r}}{\partial r} \right) - \frac{2}{3} (\nabla \cdot \vec{v}) \right] + \left[\frac{\partial \mu_t}{\partial \bar{x}} \cdot \left(\frac{\partial \bar{x}}{\partial x} \right) + \frac{\partial \mu_t}{\partial \bar{r}} \cdot \left(\frac{\partial \bar{r}}{\partial x} \right) \right] \cdot \left\{ \left[\frac{\partial v}{\partial \bar{x}} \left(\frac{\partial \bar{x}}{\partial x} \right) + \frac{\partial v}{\partial \bar{r}} \cdot \left(\frac{\partial \bar{r}}{\partial x} \right) \right] + \left(\frac{\partial u}{\partial \bar{r}} \right) \cdot \left(\frac{\partial \bar{r}}{\partial r} \right) \right\} \\
 & + (\mu + \mu_t) \cdot \left\{ \left[\frac{\partial \Omega}{\partial \bar{x}} \cdot \left(\frac{\partial \bar{x}}{\partial x} \right) + \frac{\partial \Omega}{\partial \bar{r}} \cdot \left(\frac{\partial \bar{r}}{\partial x} \right) \right] + \frac{4}{3} \frac{\partial}{\partial \bar{r}} (\nabla \cdot \vec{v}) \cdot \left(\frac{\partial \bar{r}}{\partial r} \right) \right\} \\
 & \hspace{20em} (8)
 \end{aligned}$$

4.0 A TWO-EQUATION k-ε TURBULENCE MODEL

The closure problem related to the turbulent shear stresses is handled in the present analysis through the eddy viscosity concept. The eddy viscosity (μ_t) is determined from a two-equation k-ε model through the Prandtl-Kolmogorov relation. The molecular viscosity effect, which is important in the viscous sublayer region, is modeled through the eddy viscosity coefficient (C_μ) and additional terms in turbulent kinetic energy (TKE) and dissipation equations.

The Prandtl-Kolmogorov Relation for μ_t is

$$\mu_t = \rho C_\mu \frac{k^2}{\epsilon}$$

where

$$C_\mu = \frac{A}{3(a + A/b)}, \quad A = \sqrt{2} \text{ k}\gamma\rho/\mu, \quad a = 1,100, \quad b = 0.27$$

(9)

and where k is determined from the turbulent kinetic energy equation:

$$\begin{aligned} & \left(\frac{\partial^2 k}{\partial x^2} + \frac{\partial^2 k}{\partial r^2} \right) - \frac{1}{(\mu + \mu_t)} \left(\rho u - \frac{\partial \mu_t}{\partial x} \right) \cdot \frac{\partial k}{\partial x} - \frac{1}{(\mu + \mu_t)} \cdot \left[\rho v - \frac{\partial \mu_t}{\partial r} - \delta \cdot \frac{(\mu + \mu_t)}{r} \right] \cdot \frac{\partial k}{\partial r} \\ & + \frac{\mu_t}{(\mu + \mu_t)} \left\{ 2 \left[\left(\frac{\partial u}{\partial x} \right)^2 + \left(\frac{\partial v}{\partial r} \right)^2 + \delta \cdot \left(\frac{v}{r} \right)^2 \right] + \left(\frac{\partial u}{\partial r} + \frac{\partial v}{\partial x} \right)^2 \right\} - \frac{1}{(\mu + \mu_t)} \left(\rho \epsilon + 2\mu \frac{k}{y^2} \right) \end{aligned} \quad (10)$$

and ϵ is determined from the TKE dissipation equation:

$$\begin{aligned} & \left(\frac{\partial^2 \epsilon}{\partial x^2} + \frac{\partial^2 \epsilon}{\partial r^2} \right) - \frac{1}{\left(\mu + \frac{\mu_t}{\sigma_\epsilon} \right)} \cdot \left[\rho u - \frac{\partial}{\partial x} \left(\frac{\mu_t}{\sigma_\epsilon} \right) \right] \cdot \frac{\partial \epsilon}{\partial x} - \frac{1}{\left(\mu + \frac{\mu_t}{\sigma_\epsilon} \right)} \cdot \left[\rho v - \frac{\partial}{\partial r} \left(\frac{\mu_t}{\sigma_\epsilon} \right) - \delta \cdot \frac{\left(\mu + \frac{\mu_t}{\sigma_\epsilon} \right)}{r} \right] \cdot \frac{\partial \epsilon}{\partial r} \\ & C_1 \left(\frac{\epsilon}{k} \right) \frac{\mu_t}{\left(\mu + \frac{\mu_t}{\sigma_\epsilon} \right)} \cdot \left\{ 2 \left[\left(\frac{\partial u}{\partial x} \right)^2 + \left(\frac{\partial v}{\partial r} \right)^2 + \left(\frac{v}{r} \right)^2 \cdot \delta \right] + \left(\frac{\partial u}{\partial r} + \frac{\partial v}{\partial x} \right)^2 \right\} - C_2 \rho \left(\frac{\epsilon^2}{k} \right) \frac{1}{\left(\mu + \frac{\mu_t}{\sigma_\epsilon} \right)} = 0 \end{aligned} \quad (11)$$

where

$$C_1 = 1.36, \quad C_2 = 1.92 [1 - 0.3 \exp(-R^2)], \quad R = \rho k^2 / \mu \epsilon.$$

5.0 BOUNDARY CONDITIONS AND INLET CONDITIONS

The boundary conditions for turbulent ducted flow problems can be divided into four groups, namely wall condition, symmetry condition, exit condition, and inlet condition. Of these, the inlet condition requires special attention. Therefore, it is discussed separately below. For the solid-wall boundary condition, the nonslip condition is usually used (i.e., $u = v = 0$). When a line of symmetry exists in the computational domain, a zero normal gradient condition is commonly used. At the downstream side of the computational domain, it is necessary to specify the exit conditions because of the elliptic nature of the problem. Since one does not know the exit solution in advance, a zero axial gradient condition is normally used to simulate the nearly parallel condition at the exit station.

Inlet conditions for the turbulent ducted flow problem normally consist of a core region and boundary-layer regions. The profiles in these regions usually are highly nonuniform. They can be either obtained from experiment or specified by analytical modeling. In most cases, it is not possible to obtain the complete set of data needed for computational purposes from the core region into the turbulent boundary layer-region and through the relatively thin

sublayer to the wall. Therefore, it is highly desirable to have formulae which can be used to generate a set of complete profiles for the numerical computation from some gross features of the inlet flow. In the present analysis, the inlet condition is analytically calculated on the basis of the given boundary-layer thicknesses and the Reynolds number. Within the boundary-layer region, the modified Van Driest formula is used to provide the complete profile of the velocity gradient throughout the viscous layer on the basis of an assumed total shear stress distribution (Ref. 2). The related flow variables such as velocity and stream function are derived numerically.

With a two-equation turbulence model, it is necessary to know the turbulent kinetic energy (k) and the dissipation rate (ϵ) throughout the whole turbulent boundary layer. This cannot be easily achieved experimentally. Therefore, it is computed analytically from the following TKE-shear stress relation

$$k = \frac{1}{\sqrt{C_\mu}} \frac{\mu_t}{\rho} \left(\frac{\partial u}{\partial y} \right) \quad (12)$$

where C_μ is modelled as $A/3(a + A/b)$, $A = \sqrt{2k} y/\nu$, $a = 1,100$ and $b = 0.27$. The above equation is an equation for k and y . It must be solved iteratively because of its nonlinearity. The asymptotic behavior of this relation in the region away from the thin wall layer is given by the conventional TKE-shear stress formula as

$$k = \frac{1}{0.3} \frac{\mu_t}{\rho} \left(\frac{\partial u}{\partial y} \right) \quad (13)$$

It must be emphasized again that it is very important to provide a self-consistent set of profiles so that one can avoid sudden readjustments of the numerical solution near the inlet station.

6.0 NUMERICAL METHOD AND COORDINATE TRANSFORMATION

In the present analysis, the physical flow field is first transformed into a rectangular computational domain, and the solution is obtained iteratively, with an initial flow-field guess, through a general finite-difference formulation with decay functions.

6.1 COORDINATE TRANSFORMATION

The general coordinate transformation is described in Refs. 1 and 2. In short, the domain of interest is first transformed into a rectangular region through a nonorthogonal coordinate

transformation. A second coordinate stretching is then applied to provide an adequate solution definition throughout the boundary layer, including the sublayer. In the former approach, the coordinate stretching was provided by two matched stretching functions, while in the present approach, a simple exponential coordinate stretching is employed for the boundary-layer region. The difference is in the ease of handling. In the core region, a simple uniform grid arrangement is used.

$$y = \Delta h_1 \frac{K^j - 1}{K - 1} \quad (\text{in the boundary-layer region})$$

$$\Delta y = \text{Constant} \quad (\text{in the core region}) \quad (14)$$

where y is measured normal to the wall, Δh_1 is the first mesh size, and K is the ratio between two successive mesh sizes. The first mesh size, Δh_1 , can be determined by selecting the first grid point inside the viscous sublayer at $y^+ = 2$ (i.e., $h_1 = 2 \nu/v^*$). The coefficient K must be determined iteratively when the range of y and the total number of grid points in the boundary-layer region are given.

For example, the condition is

$$y_{\max} = \frac{2\nu}{v^*} \frac{K^{JN} - 1}{K - 1} \quad (15)$$

where JN is the number of grid points which covers the range y_{\max} . The coordinate transformation factors are evaluated numerically after the transformation function is determined. The transformation function has the advantage of smoothing out the discontinuity which normally occurs at the matching points. It must be emphasized that the proper evaluation of the transformation factors is important and that the reproduction of the inlet profile can be used to check the validity of the transformation.

6.2 INITIAL FLOW-FIELD GUESS

The initial flow-field guess for the steady-state iterative procedure is very important. It affects not only the rate of convergence but also the stability of the iteration procedure. For turbulent flow computations with a low Reynolds number model, it is not known whether there is a unique path from an initially laminar region to a finally turbulent region, and vice versa. Therefore, it is important to use an initial guess with turbulence properties which are reasonably close to the final solution.

In the present approach, the inlet condition is used to obtain the initial flow-field guess. The local profile is decomposed into two parts, namely the inlet profile part and a wake profile part. These two profiles are combined to satisfy the global continuity equation (Fig. 1). For example, the velocity profile is written as

$$u = u_I(y) \frac{(u_{mean} - \Delta u)}{u_{I,c}} + \left\{ 1 + \cos \left[\frac{(y - \Delta y_1) \cdot \pi}{\Delta y_1} \right] \right\} \cdot \Delta u \quad (16)$$

At the inlet, $\Delta u = 0$ and $u_{mean} = u_{I,c}$; therefore, $u = u_I(y)$.

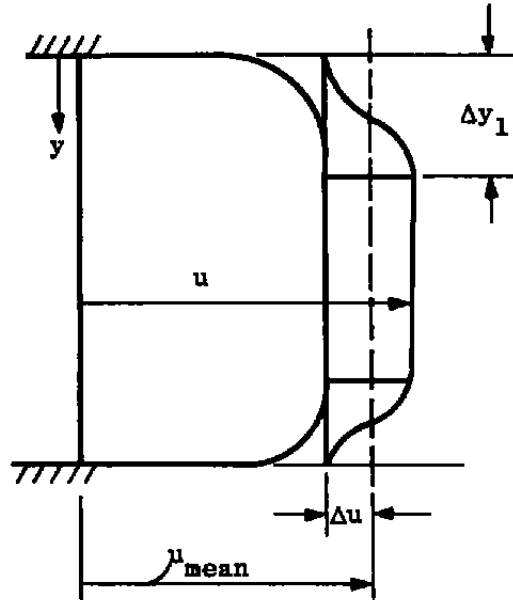


Figure 1. Decomposition of initial velocity profiles.

With the velocity profile decomposition method, the initial stream function distribution is derived. The related variables such as the vorticity and the velocity are obtained numerically. The initial viscosity distribution is computed as

$$\nu_t = \nu_{t,I} \cdot \frac{(u_{mean} - \Delta u)}{u_{I,c}} + 0.04 \cdot \Delta y_1 \cdot \Delta u \cdot \sin \left[\frac{(y - \Delta y_1) \cdot \pi}{\Delta y_1} \right] \quad (17)$$

where the first term represents the contribution from the adjusted inlet condition and the second term represents the corresponding wake contribution; Δy_1 is the assumed local boundary-layer thickness. Improvement in the initial flow-field guess could be further carried out by combining experimental data, computed results, and a simple integral method to make the Navier-Stokes computer code "smart."

6.3 NUMERICAL SOLUTION PROCEDURE

The governing equations and the corresponding boundary conditions are solved in the transformed space by a general finite-difference method with decay functions (Refs. 5 and 6). The program logic for the incompressible flow computation is shown in Fig. 2. The vorticity and the stream function equation form a main loop along with the eddy viscosity computation. The pressure equation forms another separate loop because of the pressure decoupling mechanism in incompressible flow.

For the compressible flow computation, the vorticity, stream function, eddy viscosity, energy, and pressure equations form a main loop (Fig. 3). The pressure field must be updated constantly because of the density coupling in the compressible flow. Basically, the compressibility effect appears in the convection term because of the density modification.

7.0 RESULTS AND DISCUSSION

The application of the general finite-difference method with decay functions to the solution of the Navier-Stokes equations in terms of the vorticity-stream function formulation is new. Therefore, it is very important to know the validity and the limitation of this approach. In previous work (Refs. 1 and 2) it was studied very carefully and was applied to the laminar diffuser flow computations, where the numerical solution can be easily verified without the complication of turbulence modeling. With the coordinate stretching, the technique was applied to the computation of incompressible 2-D planar diffuser flows and several separated and nonseparated conical diffuser flows. The results, by comparison with a limited amount of available data, were encouraging. Obvious extensions to the previous work were 1) to include more complicated boundaries, such as annular diffusers, and 2) to account for compressibility effects. To evaluate the first extension, the analysis and the computer code were applied to a wind tunnel diffuser with centerbody. To answer the question about compressibility, several steps were taken. These are described in the following sections.

7.1 INCOMPRESSIBLE WIND TUNNEL DIFFUSER FLOW COMPUTATION

The wind tunnel diffuser modeled is part of the AEDC Propulsion Wind Tunnel Facility (PWT) Aerodynamic Wind Tunnel (16T). The outer wall of the diffuser is three-dimensional. A square inlet section is followed by a transition section which changes the cross section from square to circular (Fig. 4). The diffuser centerbody is axisymmetric. The computations were made for an equivalent axisymmetric annular diffuser which has the same axial distribution of flow area as the actual diffuser. The computed flow field can be expected to be significantly in error in those parts of the diffuser where the cross section of the outer wall deviates greatly from axisymmetric. However, if the predicted flow field is in

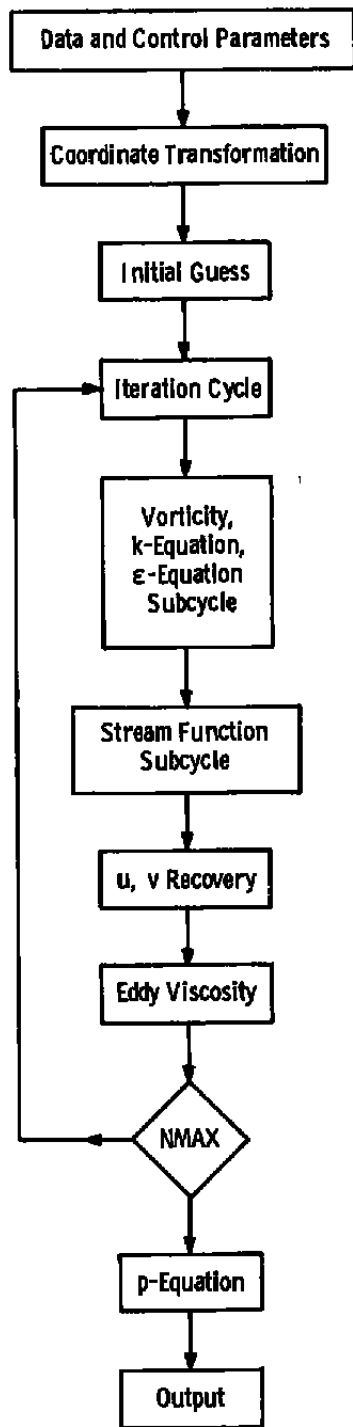


Figure 2. Flow chart for incompressible flow solution procedure.

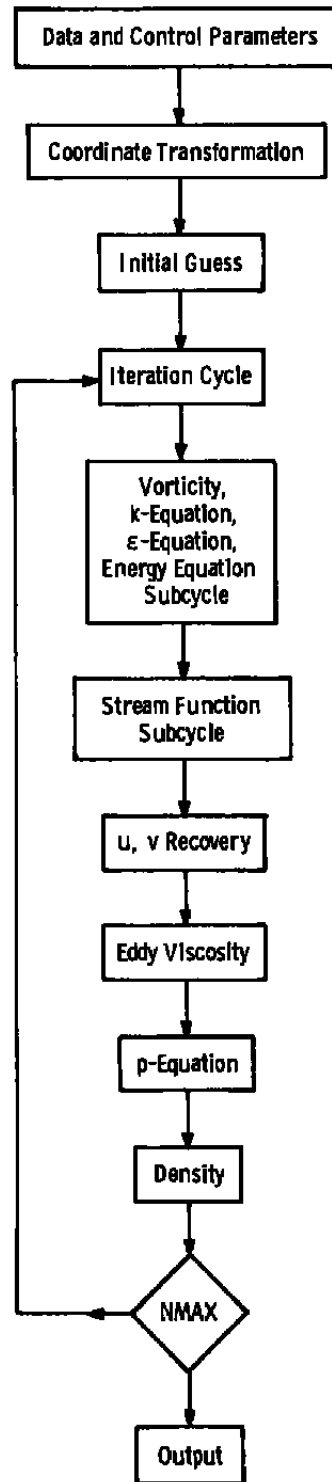


Figure 3. Flow chart for compressible flow solution procedure.

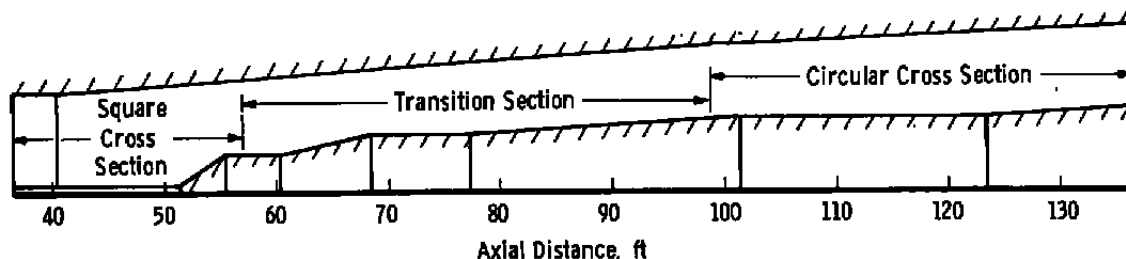
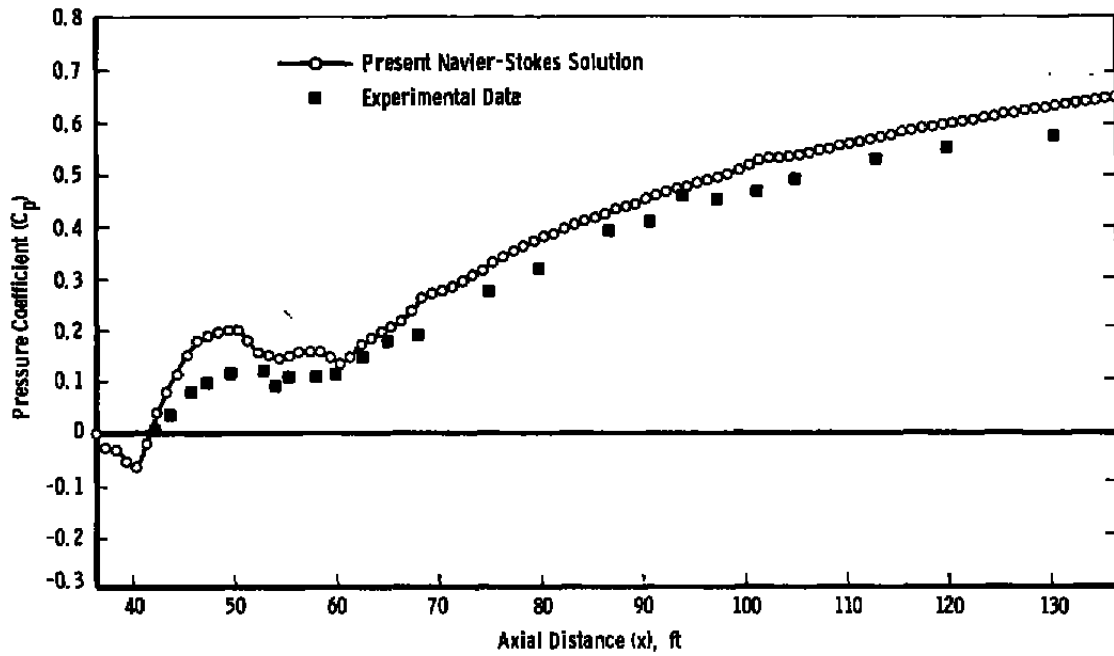


Figure 4. 16T diffuser geometry.

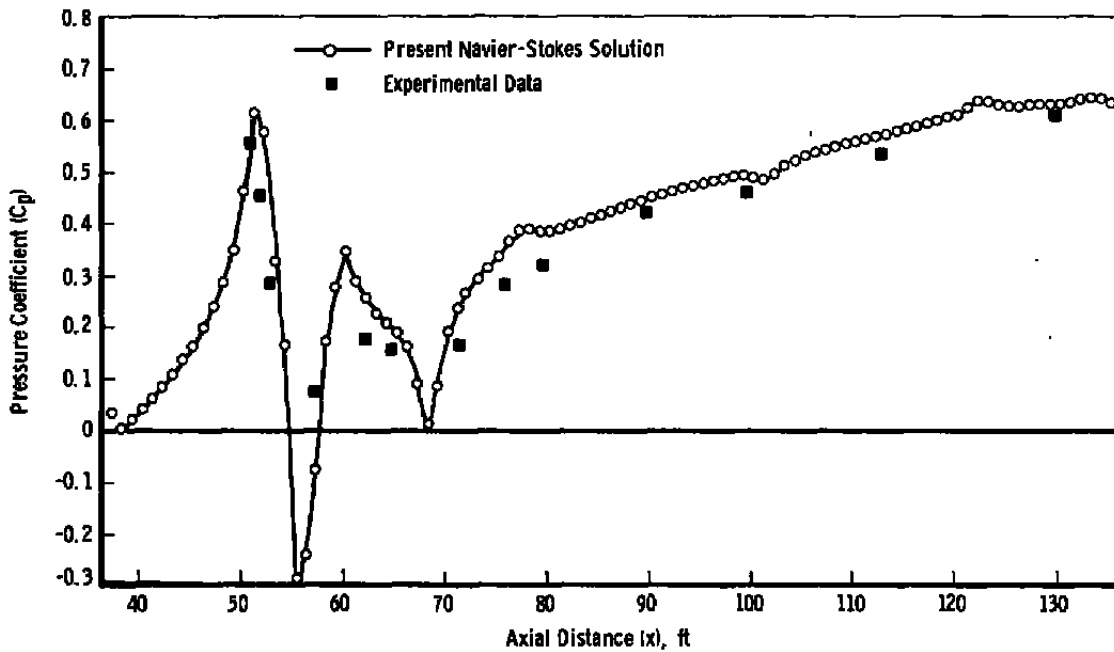
reasonable agreement with experiment, then the numerical computations can be used to assess the effect of geometric and Reynolds number variations on the performance of the 16T diffuser.

In the course of this analysis a completely new formulation was carried out to include both the wall and the centerbody turbulent boundary layers. Unfortunately, this placed a very heavy demand on the coordinate transformation, because it meant that one must handle two viscous layers, two sublayers, and a core region. The two-function matching procedure proved to be insufficient to provide a smooth and continuous transformation in the realistic Reynolds number range of 4×10^6 with about 61 grid points in the radial direction. This problem was later solved with a simple exponential function transformation which is described in Section 5.1. With this approach, the core region was handled by a uniform grid, and the two boundary layers were covered by a two-exponential function transformation.

In the computation, a 69 by 105 grid was generated in the radial and axial directions. In the radial direction, the two boundary layers along the outer diffuser wall and the centerbody were covered by the grid. The centerbody was extended to the inlet plane with a small sting to eliminate the direct computation of the stagnation point region of the centerbody. The computed wall and the centerbody pressure coefficients are shown in Fig. 5. Also in Fig. 5, experimental results are presented from a 1/16 scale model of the diffuser tested in the AEDC-PWT Aerodynamic Wind Tunnel (1T). Agreement with 1T model data is good except for the wall pressure in the square inlet section, where large three-dimensional effects exist. The Reynolds number per foot is 4×10^6 . The computations required approximately one hour on an IBM 370/165 computer. The storage requirement with double precision is about 1.2×10^6 bytes. From the convergence history shown in Fig. 6, it can be seen that the solution reached a converged state in about 30 minutes. The pressure distribution was obtained from the new pressure equation. The convergence history with the new equation is shown in Fig. 7. It can be seen that the convergence is relatively fast compared to the vorticity-stream function cycle. This is very important because the pressure cycle must be updated constantly in the future computation of compressible flows.



a. Wall C_p distribution



b. Scoop (centerbody) C_p distribution
 Figure 5. C_p distribution for 16T model diffuser.

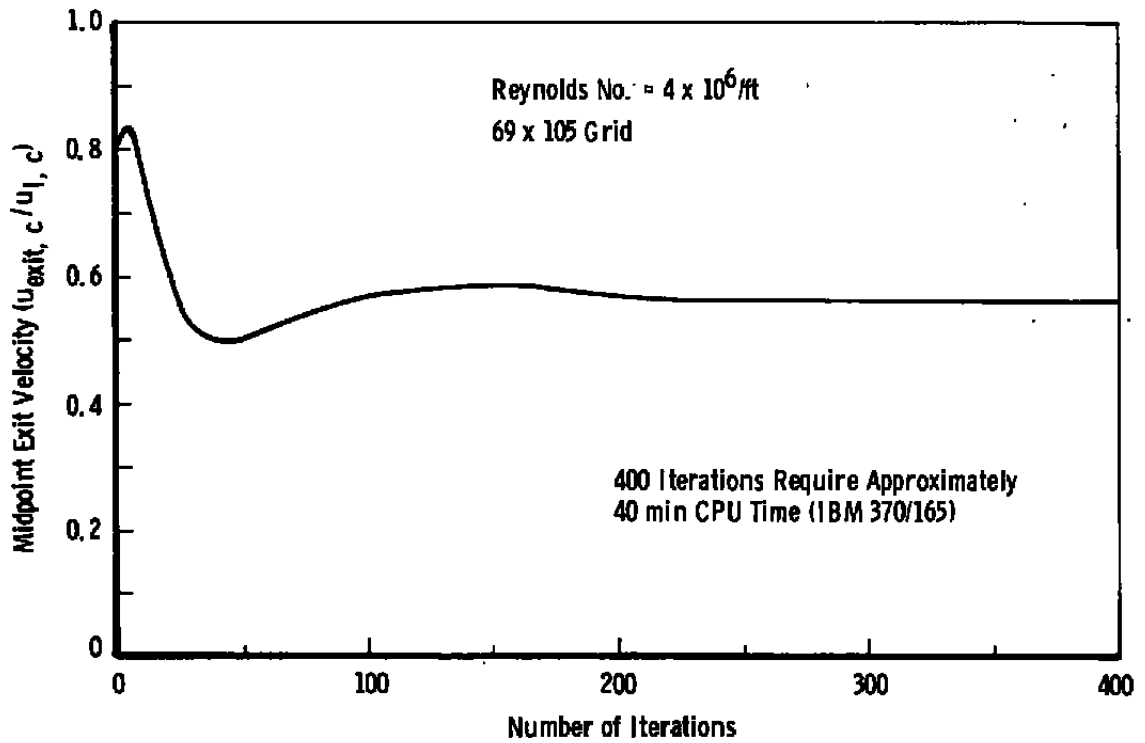


Figure 6. Convergence characteristics for 16T model diffuser computation.

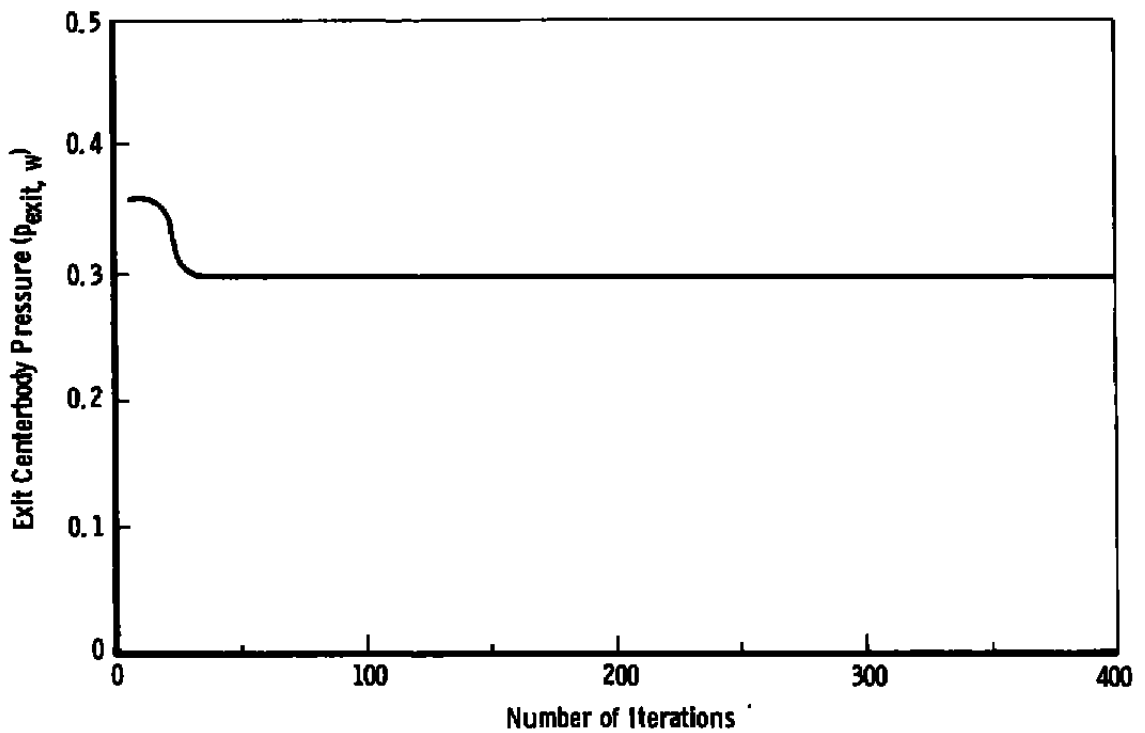


Figure 7. Convergence characteristics for the new pressure equation.

Obviously the ability to efficiently obtain accurate pressure distributions with the new method has been successfully demonstrated. Finally, it is worthwhile to mention that these computations were carried out with a uniform axial mesh arrangement, which may not be adequate for flows with large variation in geometry along the axial direction. Therefore, extension to include a variable mesh in the axial direction is also desirable.

Although only the pressure distributions are presented here, a complete set of flow-field variables was tabulated as the output of the computer code.

7.2 COMPRESSIBLE LAMINAR FLOW IN A SUDDEN EXPANSION DIFFUSER

Although the vorticity-stream function formulation has been very successful in handling incompressible two-dimensional flow problems, the capability of this approach to obtain compressible flow solutions must be demonstrated. The reason behind this is that it becomes necessary to update the pressure constantly by solving a pressure equation. The old problem associated with the conventional pressure equation (i.e., slow convergence and boundary condition) has discouraged people from using it. It is therefore very important to select a well-defined and physically realistic test case so that the present logic for the compressible flow can be verified. For this reason, the planar laminar flow in a sudden expansion diffuser was chosen to eliminate the additional complication involved in the use of the $k-\epsilon$ turbulence model.

The velocity profile is shown in Fig. 8. At the inlet, the Mach number in the core region is 0.8, and there is a laminar boundary layer near the wall. The computation was started at one step height (H) ahead of the expansion so that the elliptic nature of the flow could be properly included. The flow separates smoothly from the corner and forms a long separation region. For a Reynolds number equal to 70, the length of the recirculation region is about $7.5H$. The centerline velocity also decreases continuously because of the diffusion process.

In the computation, the conventional pressure equation of the Poisson type was used. It is likely that one can include the new pressure equation in the analysis and modify the computer code to obtain accurate pressure distributions in a more efficient way. The convergence characteristics are shown in Fig. 9 with the conventional pressure equation. The grid arrangement is a 101 by 36 uniform mesh, and the computing time was about 8.5 min.

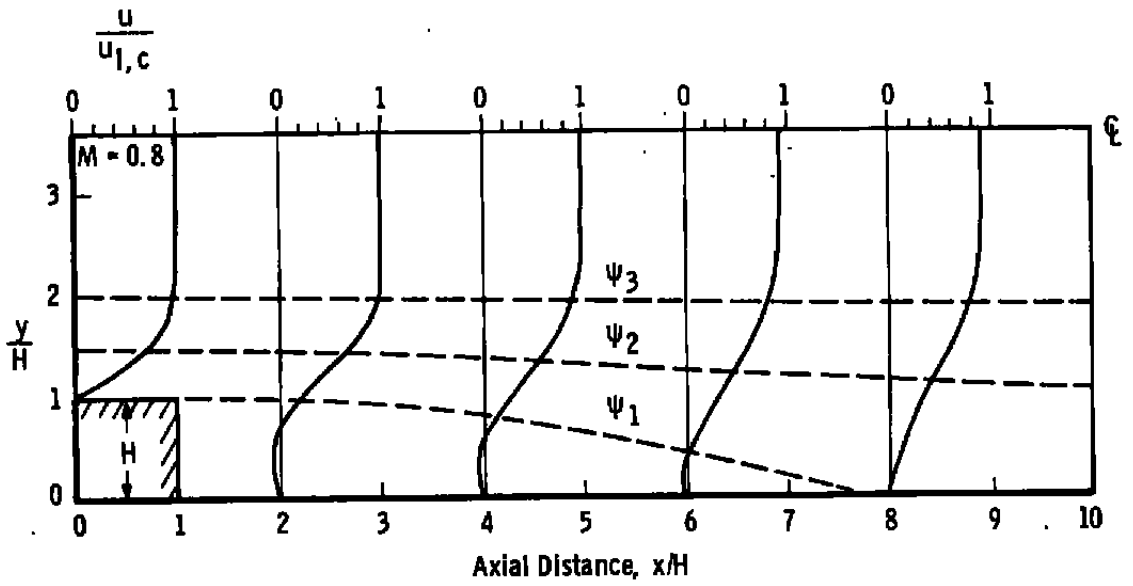


Figure 8. Velocity and streamline distribution of a sudden expansion diffuser.

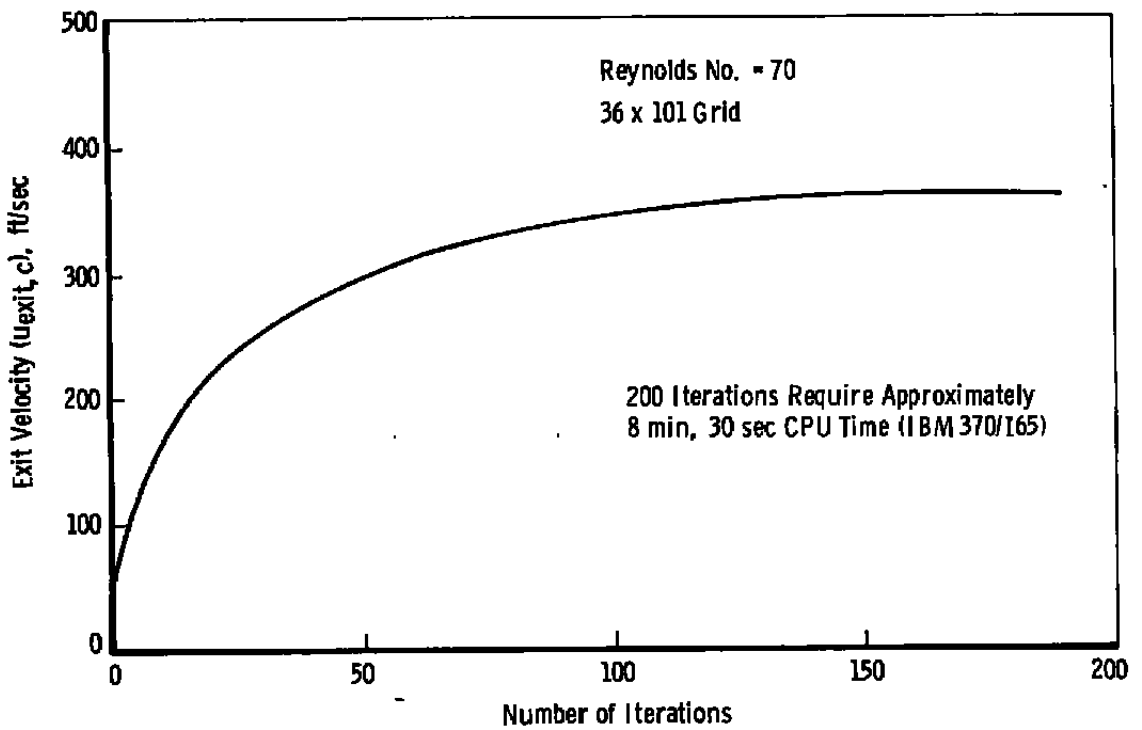


Figure 9. Convergence characteristics of sudden expansion diffuser computation.

8.0 CONCLUDING REMARKS

The present steady-state vorticity-stream function formulation has been shown to provide convergent solutions for both compressible and incompressible internal flows. The new pressure equation derived also provides fast and accurate pressure distributions for the fairly complicated 16T model diffuser configuration. The full potential of the present formulation should be further validated for the Mach number effect when additional data for the 16T model diffuser are obtained. The extension to three-dimensional flows also should be carried out with a vorticity-velocity formulation because most flow problems are three-dimensional in nature.

REFERENCES

1. Chien, J. C. "Numerical Analysis of Turbulent Separated Subsonic Diffuser Flows." AEDC-TR-76-159 (ADA036005), February 1977.
2. Chien, J. C. "Numerical Computation of Subsonic Conical Diffuser Flows with Nonuniform Turbulent Inlet Conditions." AEDC-TR-77-78 (ADA044948), September 1977.
3. Gosman, A. D., Pun, W. K., Runchael, A. K., Spalding, D. B., and Wolfshtein., M. *Heat and Mass Transfer in Recirculating Flows*. Academic Press, New York 1969.
4. Schulz, R. J. "Numerical Analysis of Recirculating Ducted Flows." AEDC-TR-78-29 (ADA062945), December 1978.
5. Chien, J. C. "A General Finite-Difference Formulation with Application to Navier-Stokes Equations." *Journal of Computational Physics*, Vol. 20, No. 3, March 1976, pp. 268-278.
6. Chien, J. C. "A General Finite-Difference Formulation with Application to Navier-Stokes Equations." *Computers and Fluids*, Vol. 5, No. 1, March 1977, pp. 15-31.

NOMENCLATURE

A	Variable, $= \sqrt{2k} y/\nu$
a, b	Constants
C	Coefficient in the eddy viscosity model
C_p	Pressure coefficient
H	Step size
Δh₁	First step size
j	Integer
K	Coordinate transformation constant
k	Turbulent kinetic energy (TKE)
M	Mach number
P1, P2	Vector path function
p	Pressure
p_{exit, w}	Exit wall pressure
R	Gas constant
r	Radial coordinate
S_p	Pressure source term
T	Temperature
u, v	Axial and radial velocity components
Δu	Wake component in velocity profile
u_c	Reference velocity
u_{exit,c}	Exit reference velocity
u_{l,c}	Inlet reference velocity

u_{mean}	Mean velocity
v^*	Friction velocity
x	Axial coordinate
y	Normal coordinate
Δy	Step size in y
Δy_1	Boundary-layer thickness
δ	2-D flow, = 0; axisymmetric flow, = 1
ϵ	TKE dissipation
μ	Molecular viscosity
μ_t	Eddy viscosity
ν_t	Eddy viscosity divided by density (μ_t/ρ)
ρ	Density
ψ	Stream function
Ω	Vorticity